

Dynamic fluctuations in the superconductivity of NbN films from microwave conductivity measurements

Takeyoshi Ohashi, Haruhisa Kitano, and Astutaka Maeda
*Department of Basic Science, The University of Tokyo,
 3-8-1, Komaba, Meguro-ku, Tokyo 153-8902, Japan*

Hiroyuki Akaike and Akira Fujimaki
*Department of Quantum Engineering, Nagoya University,
 Furocho, Chikusa-ku, Nagoya-shi, Aichi, 464-8603, Japan*
 (Dated: January 7, 2022)

We have measured the frequency and temperature dependences of complex ac conductivity, $\sigma(\omega) = \sigma_1(\omega) - i\sigma_2(\omega)$, of NbN films in zero magnetic field between 0.1 to 10 GHz using a microwave broadband technique. In the vicinity of superconducting critical temperature, T_c , both $\sigma_1(\omega)$ and $\sigma_2(\omega)$ showed a rapid increase in the low frequency limit owing to the fluctuation effect of superconductivity. For the films thinner than 300 nm, frequency and temperature dependences of fluctuation conductivity, $\sigma_{\text{fl}}(\omega, T)$, were successfully scaled onto one scaling function, which was consistent with the Aslamazov and Larkin model for two dimensional (2D) cases. For thicker films, $\sigma_{\text{fl}}(\omega, T)$ data could not be scaled, but indicated that the dimensional crossover from three dimensions (3D) to 2D occurred as the temperature approached T_c from above. This provides a good reference of ac fluctuation conductivity for more exotic superconductors of current interest.

PACS numbers: 74.25.Nf, 74.40.+k, 74.70.Ad, 74.78.-w

Keywords: superconductivity, fluctuation, microwave conductivity, dynamic scaling, NbN

I. INTRODUCTION

The effects of thermal fluctuation near the superconducting phase transition have been an interesting issue for many years, both theoretically and experimentally [1]. These effects attract much attention particularly for strongly type-II superconductors of recent interest, for example, the high- T_c cuprate superconductors, the organic superconductors, and the heavy Fermion superconductors, because the effects of thermal fluctuation are enhanced by the short coherence length and the anisotropy [2].

The superconducting fluctuation leads to a divergence of a number of physical quantities, such as, the specific heat, the susceptibility, the dc nonlinear electrical conductivity, and the ac linear electrical conductivity. One of the remarkable features of the superconducting fluctuation is a scaling behavior appearing in these diverging quantities. Detailed analyses of such scaling behavior provide important information on the universality class of the second order phase transition. Among these physical quantities, ac conductivity is one of the most powerful probes to investigate the fluctuation effect, because the frequency and temperature dependences of complex conductivity enable the direct verification of a dynamic scaling theory [3]. Although the theory predicts the scaling behavior in other dc quantities, as well as in the frequency dependence of the ac conductivity, $\sigma(\omega)$, the latter has an additional advantage. The scaling analysis generally needs two scaling parameters to be determined. It is, however, impossible to determine these two parameters uniquely from the dc (not complex) experimental data. Therefore, the scaling analyses of dc data usually assume

a particular dimension in order to establish a certain relationship between these two parameters. This reduces the degrees of freedom in the scaling analyses from two to one, leading to less convincing analyzed results. Contrary to this, complex $\sigma(\omega)$ can provide the unique determination of the scaling parameters without any assumptions.

Recently, the dynamic scaling analyses on ac conductivity have been performed for some kinds of high- T_c cuprates. Booth *et al.* [4] investigated optimally doped YBa₂Cu₃O_{7- δ} thin films by microwave measurement and observed a critical fluctuation with a large dynamic critical exponent, $z \sim 2.3 - 3.0$. Corson *et al.* [5] investigated underdoped Bi₂Sr₂CaCu₂O_{8+ δ} thin films by THz techniques and observed thermally generated vortices, which are explained in the 2D-XY model. In spite of these studies, a general consensus on the fluctuation of high- T_c cuprates has not yet been achieved. This is, in part, due to the lack of systematic studies on high- T_c cuprates and fundamental studies on conventional superconductors which are very important as reference results for many more exotic superconductors of recent interest. Previous studies on the ac fluctuation conductivity of conventional superconductors have been published. For instance, Lehoczký and Briscoe [6] measured the temperature dependence of fluctuation conductivity on lead films at several fixed microwave frequencies. Tanner [7] measured the temperature dependence of the characteristic frequency of the fluctuation on lead films by far-infrared transmission. Although these studies were in agreement with the calculation on Gaussian theory [8], the frequency dependence was insufficient to examine the scaling analysis. In addition, these studies compared the measured conductivity or some other physical quantities

with the theoretical prediction based on a particular microscopic model. In contrast, dynamic scaling analysis works without any explicit calculations of the individual models. This is the most significant merit of dynamic scaling. However, there are no studies of dynamic scaling analysis of ac fluctuation conductivity on conventional superconductors in zero magnetic field, though this approach has been applied to the vortex-glass transition in conventional superconductor, indium [9].

In this paper, we report the frequency and temperature dependences of ac conductivity of films of a conventional superconductor, NbN, and perform dynamic scaling analysis on excess conductivity due to the superconducting fluctuation effects in zero magnetic field. The comprehensive examinations of the fluctuation conductivity, including the scaling behavior itself, critical exponents, and also the explicit temperature and frequency dependences of fluctuation conductivity, clarify the validity and the limit of the dynamic scaling analysis.

II. SUMMARY OF THEORETICAL BACKGROUND

The first successful theory of the dc fluctuation conductivity in superconductors was provided by Aslamazov and Larkin [10]. They considered the thermal relaxation of the order parameter to calculate the direct contribution of the superconducting pairs created by fluctuations (AL-term), as follows,

$$\begin{aligned}\sigma_{\text{dc}}^{2\text{DAL}} &= \frac{1}{16} \frac{e^2}{\hbar t} \varepsilon^{-1}, \\ \sigma_{\text{dc}}^{3\text{DAL}} &= \frac{1}{32} \frac{e^2}{\hbar \xi_0} \varepsilon^{-1/2},\end{aligned}\quad (1)$$

where t is the thickness, ξ_0 is the coherence length at 0 K, and $\varepsilon = |T/T_c - 1|$. These predictions were in good agreement with experimental results on dirty superconductors [11]. Maki [12] and Thompson [13] proposed the existence of an additional term (MT-term) owing to an indirect contribution of the superconducting fluctuation on the quasiparticle conductivity, as follows,

$$\begin{aligned}\sigma_{\text{dc}}^{2\text{DMT}} &= \frac{1}{8} \frac{e^2}{\hbar t} \frac{1}{\varepsilon - \delta} \ln \left(\frac{\varepsilon}{\delta} \right), \\ \sigma_{\text{dc}}^{3\text{DMT}} &= \frac{1}{8} \frac{e^2}{\hbar \xi_0} \varepsilon^{-1/2},\end{aligned}\quad (2)$$

where δ is the pair-breaking parameter introduced to avoid an unphysical divergence of conductivity at $T > T_c$ in the 2D case. The MT term explained a larger magnitude and an anomalous temperature dependence of the fluctuation conductivity observed on cleaner superconductors [14, 15].

As for the dynamic aspect of the fluctuation, the frequency dependence of the AL-term was calculated by Schmidt [8] using the time-dependent Ginzburg-Landau equation, as follows,

$$\begin{aligned}\sigma^{2\text{DAL}}(\omega) &= \sigma_{\text{dc}}^{2\text{DAL}} S^{2\text{DAL}} \left(\frac{\pi \hbar \omega}{16 k_B T_c \varepsilon} \right), \\ \text{Re} S^{2\text{DAL}}(x) &= \frac{2}{x} \tan^{-1} x - \frac{1}{x^2} \ln(1 + x^2), \\ \text{Im} S^{2\text{DAL}}(x) &= \frac{2}{x^2} (\tan^{-1} x - x) + \frac{1}{x} \ln(1 + x^2), \\ \sigma^{3\text{DAL}}(\omega) &= \sigma_{\text{dc}}^{3\text{DAL}} S^{3\text{DAL}} \left(\frac{\pi \hbar \omega}{16 k_B T_c \varepsilon} \right), \\ \text{Re} S^{3\text{DAL}}(x) &= \frac{8}{3x^2} \left[1 - (1 + x^2)^{3/4} \cos \left(\frac{3}{2} \tan^{-1} x \right) \right], \\ \text{Im} S^{3\text{DAL}}(x) &= \frac{8}{3x^2} \left[-\frac{3}{2} x + (1 + x^2)^{3/4} \sin \left(\frac{3}{2} \tan^{-1} x \right) \right].\end{aligned}\quad (3)$$

On the other hand, the frequency dependence of the MT-term was calculated by Aslamazov and Varlamov [16]. Starting from a layered superconductor they found, in

the 2D and 3D limits, that the contribution of the MT-term should be added to the AL-term, as follows,

$$\begin{aligned}
\text{Re}S^{2\text{DAL}+\text{MT}}(x) &= \text{Re}S^{2\text{DAL}}(x) + \frac{2\pi x - 2 \ln 2x}{1 + 4x^2}, \\
\text{Im}S^{2\text{DAL}+\text{MT}}(x) &= \text{Im}S^{2\text{DAL}}(x) + \frac{\pi + 4x \ln 2x}{1 + 4x^2}, \\
\text{Re}S^{3\text{DAL}+\text{MT}}(x) &= \text{Re}S^{3\text{DAL}}(x) + \frac{4 - 4x^{1/2} + 8x^{3/2}}{1 + 4x^2}, \\
\text{Im}S^{3\text{DAL}+\text{MT}}(x) &= \text{Im}S^{3\text{DAL}}(x) + \frac{4x^{1/2} - 8x + 8x^{3/2}}{1 + 4x^2}.
\end{aligned} \tag{4}$$

The appearance of the high- T_c cuprate superconductors enabled us to recognize importance of the critical fluctuation even in the physics of superconductivity. It is expected that higher T_c , shorter coherence length, longer magnetic penetration depth, and quasi-two dimensionality enhance the temperature region where the Gaussian theory is not valid. To study such a critical region, Fisher, Fisher and Huse [2] formulated a dynamic scaling rule on fluctuation conductivity in the vicinity of a second order phase transition, as follows,

$$\sigma_{\text{fl}}(\omega) = \sigma_0 S\left(\frac{\omega}{\omega_0}\right), \tag{5}$$

where S is a complex universal scaling function, and σ_0, ω_0 are scaling parameters whose temperature dependences are related to that of a correlation length, ξ , which diverges at T_c , as follows,

$$\begin{aligned}
\sigma_0(\varepsilon) &\propto [\xi(\varepsilon)]^{z+2-d}, \\
\omega_0(\varepsilon) &\propto [\xi(\varepsilon)]^{-z}, \\
\xi(\varepsilon) &= \xi_0 \varepsilon^{-\nu},
\end{aligned} \tag{6}$$

where ν is a static critical exponent, z is a dynamic critical exponent, and d is an effective spatial dimension. In the limit of $\omega/\omega_0 \rightarrow \infty$, $\sigma_{\text{fl}} = |\sigma_{\text{fl}}|e^{i\phi_{\text{fl}}}$ behaves as

$$\begin{aligned}
|\sigma_{\text{fl}}|(\omega) &\propto \omega^{-(z+2-d)/z}, \\
\phi_{\text{fl}}(\omega) &= \frac{\pi}{2} \frac{z+2-d}{z}.
\end{aligned} \tag{7}$$

Thus, keeping these formulas in mind, ν , z , and d can be obtained by the $\sigma_{\text{fl}}(\omega, T)$ measurement, and the universality class of the transition can be determined.

Note that this scaling theory is a general one which also contains the Gaussian result as a special case; $z = 2, \nu = 0.5$ [17]. In this case, the scaling functions are exactly the same as given in Eqs. (3) and (4). The Gaussian results of the scaling functions are shown in Fig 1.

III. EXPERIMENTAL

A. Fabrication and characterization of NbN films

NbN films were deposited on LaSrAlO₄(LSAO) (001) substrate by a reactive sputtering technique, details of

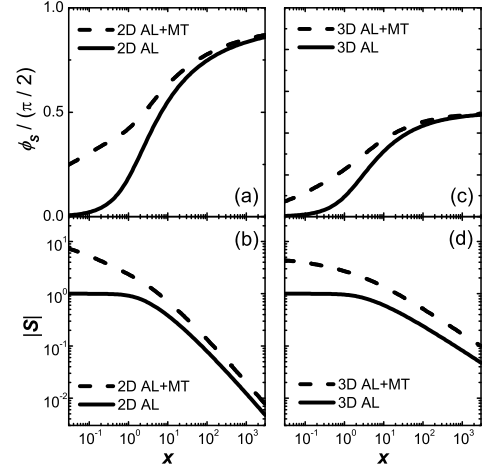


FIG. 1: Phase, $\phi_S(x)$, and amplitude $|S(x)|$ of theoretical scaling functions for the AL term and the AL term + the MT term for (a),(b) the 2D and (c),(d) the 3D case.

which were described elsewhere [18]. The thicknesses of prepared films, t 's, were 50 nm, 150 nm, 300 nm, and 450 nm, respectively. NbN was a suitable reference for high- T_c cuprates because its short coherence length (2 - 4 nm) and long penetration depth (200 - 600 nm) [19, 20, 21], are relatively similar to those of high- T_c cuprates. We selected LSAO substrates for the direct comparison of NbN data with those of La_{2-x}Sr_xCuO₄ epitaxial thin films on LSAO [22].

Figure 2(a) shows the dc resistivity, ρ , of the film with 300 nm measured by an ordinary four-probe method. The resistive critical temperatures, T_c^R , were defined as the temperature at which dc resistivity vanishes, and the electronic mean free paths, l , were estimated using the relationship, $l = 9 \times 10^{11} \hbar (3\pi^2)^{1/3} [e^2 \rho (n^{2/3} \times 0.6)]^{-1}$, where we used the carrier concentration $n \approx 2.4 \times 10^{23} \text{ cm}^{-3}$ and the ratio of the area of the Fermi surface to that of a free-electron Fermi surface ~ 0.6 [19]. They are listed in Table I, together with some important parameters. As shown in the inset of Fig. 2(a), T_c^R decreased linearly with the sheet resistance, R_{\square} . This sheet resistance dependence was consistent with a prediction by

TABLE I: Various parameters of the NbN films; t : thickness, ρ : dc resistivity, R_{\square} : sheet resistance, T_c^R : the resistive T_c , T_c^{MF} : the mean-field T_c , T_c^{scale} : the T_c used for the scaling analysis, ξ_0 : the coherence length at 0 K, l : the electronic mean free path, and ε_c : the crossover temperature from 3D to 2D. See the text for details.

t (nm)	ρ (m Ω cm)	R_{\square} (Ω)	T_c^R (K)	T_c^{MF} (K)	T_c^{scale} (K)	ξ_0 (nm)	l (nm)	ε_c
50	0.27	54	12.81	12.87	12.865	3.6	0.20	5.1×10^{-2}
150	0.20	20	14.24	14.36	14.360	3.9	0.27	6.7×10^{-3}
300	0.19	6.3	14.89	14.90	-	4.1	0.29	1.8×10^{-3}
450	0.22	4.9	15.09	15.12	-	4.2	0.25	8.6×10^{-4}

a theory of weak localization [23], indicating that a series of these films was sufficiently uniform to discuss the thickness dependence.

As shown in Fig. 2(b), we also measured dc resistivity under dc magnetic fields applied parallel to the film in order to estimate the upper critical field, B_{c2} . Using the relationships $B_{c2}(0) \approx 0.7d B_{c2}(T)/dT|_{T=T_c}$ [24] and $\xi_0 = (\Phi_0/2\pi B_{c2}(0))^{1/2}$, where Φ_0 is the flux quantum, ξ_0 was evaluated, which is also listed in Table I. All the films satisfied the condition, $l \ll \xi_0$, guaranteeing that they are in the dirty limit.

B. Microwave broadband method for ac conductivity measurement

We measured the complex reflection coefficient, S_{11} , of the film placed at the end of the transmission line. Since this is a non-resonant method that is free from the frequency restriction of resonant methods, the detailed frequency dependence can be obtained. The complex impedance, Z_L , and the complex conductivity, σ , of the sample can be obtained from S_{11} , as follows [25],

$$Z_L = \frac{1 + S_{11}}{1 - S_{11}} Z_0,$$

$$Z_L = \sqrt{\frac{i\mu\omega}{\sigma}} \coth(\sqrt{i\mu\omega\sigma}t), \quad (8)$$

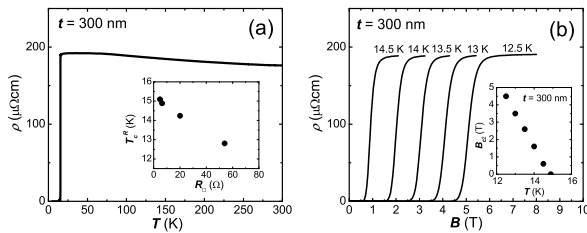


FIG. 2: (a) Temperature dependence of dc resistivity, ρ , of the NbN film with $t = 300$ nm. Inset: Sheet resistance dependence of T_c^R . (b) Magnetic field dependence of dc resistivity, ρ , of the NbN film with $t = 300$ nm. Inset: Temperature dependence of B_{c2} .

where $Z_0 = 377 \Omega$ is the impedance of free space, and μ is a permeability, which can be approximated by that of vacuum in this paper. When t is much less than the skin depth of the sample ($\sim 10 \mu\text{m}$ for NbN at 10 GHz), Eq. (8) can be approximated as follows,

$$Z_L = \frac{1}{t\sigma}. \quad (9)$$

Therefore, σ can be derived directly from S_{11} for sufficiently thin films. This is one reason why we used films in this study.

Equation (8) shows that even a small error in S_{11} can have a large effect on the calculation of σ , particularly when Z_L is much smaller than Z_0 . In practice, a condition, $|Z_L| > 0.2 \Omega$, is required because the error in $|S_{11}|$ is about 0.01 dB and $Z_L = 0.2 \Omega$ corresponds to $|S_{11}| = -0.01$ dB. The typical normal resistivity of NbN is $200 \mu\Omega\text{cm}$. Thus, only films thinner than $1 \mu\text{m}$ satisfy this condition, if we tend to measure $\sigma(\omega)$ in the vicinity of T_c , where $|Z_L|$ is 10 times lower than in the normal state.

C. Measurement setup

The microwave broadband method is a two-probed measurement affected by the contact resistance. To reduce the contact resistance, gold electrodes 200 nm thick were sputtered on the surface of the films and annealed in air at 250 °C for 1 hour. The electrodes in the samples for microwave measurement were made into the so-called Corbino-disk geometry. The diameters of the inner and outer electrodes were 1.0 mm and 2.4 mm, respectively.

The film was connected to a coaxial cable (RG 405/U) through a modified 2.4 mm jack-to-jack coaxial adapter (M/A-COM OS-2.4 adaptor 8580-0000-02). A spring-loaded gold pin in the center conductor of the modified adapter and a spring set behind the substrate made a stable electrical contact between the sample and the transmission line even at low temperatures [25, 26]. The other end of the transmission line was connected to a vector network analyzer (HP8510C) to measure S_{11} over the frequency range from 45 MHz to 50 GHz. The network analyzer was operated in the step-sweep mode to ensure the phase coherence at each frequency. The inner and outer conductors of the coaxial cable were made of Cu except for the last 15 cm in the neighborhood of the

sample, where CuNi was used to reduce the thermal flow into the sample. The length of the whole transmission line was ~ 1.7 m and its loss was ~ 5 dB at 10 GHz. Incident microwave power was 0 dBm, so that the amplitude of the current density in the film was $\sim 1000 \text{ Acm}^{-2}$. S_{11} did not show the incident power dependence at this power range for $T > T_c$ indicating that the linear conductivity was measured. We also measured dc resistance, R , just before and after the measurement of $S_{11}(\omega)$, by connecting a dc current source and a voltmeter to the transmission line through the bias port of the network analyzer.

All measurements were performed after keeping the sample holder in the cryostat at least for 10 hours in order to ensure the equilibrium of temperature distribution in the transmission line. During each measurement, the temperature was fixed to a constant value within ± 1 mK.

D. Calibration

The experimentally measured reflection coefficient includes the extrinsic attenuation, reflection, and phase shift due to the transmission line *etc.* This problem becomes more complicated for measurements at low temperatures, because the conductivity and the length of the transmission line considerably vary with temperature.

To calibrate, we performed the following procedure at each frequency and temperature. The measured reflection coefficient, S_{11}^m , can be expressed as follows,

$$S_{11}^m = E_D + \frac{E_R S_{11}}{1 - E_S S_{11}}, \quad (10)$$

where E_D , E_R , and E_S are complex error coefficients representing the directivity, the reflection tracking, and the source mismatch, respectively [27]. Equation (10) implies that a set of three independent measurements using loads with known Z_L (or S_{11}) are needed to determine three error coefficients [28]. Once they are obtained, all systematic errors can be eliminated from S_{11}^m data, utilizing Eq. (10). However, all errors are not completely systematic nor reproducible, because there are small differences in the experimental configurations among different measurement runs for the sample and the known loads. This becomes serious, especially in measurements of samples with small impedance. To overcome this difficulty, we regard the $|S_{11}|(\omega)$ of the sample in the superconducting state at 10 K (the lowest temperature of the measurement) to be equal to that of an ideal short ($Z_L(\omega) = 0$), and $S_{11}(\omega)$ of the normal state at 20-25 K (the temperatures sufficiently far from the fluctuation region) to that of an ideal load ($Z_L(\omega) = R(\omega = 0)$). This assumption is reasonable because (1) the expected loss of NbN at 10 K ($\sim 10^{-5}$ dB) is much less than the resolution of our measurement, (2) the Drude relaxation rate of NbN ($\sim 10^{14} \text{ s}^{-1}$ [29]) is much higher than the measured frequency, and (3) the change in the property of the transmission

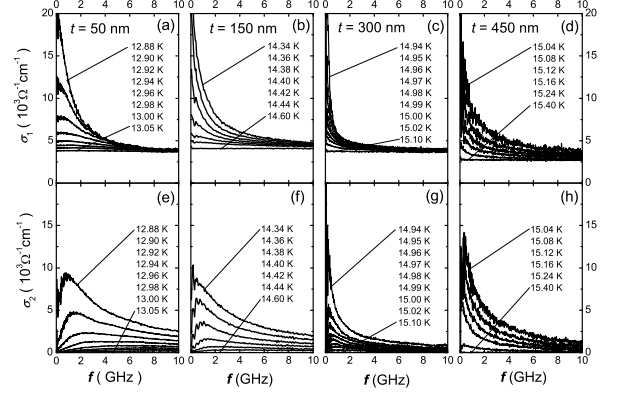


FIG. 3: Frequency dependence of (a)-(d) σ_1 and (e)-(h) σ_2 at several temperatures near T_c

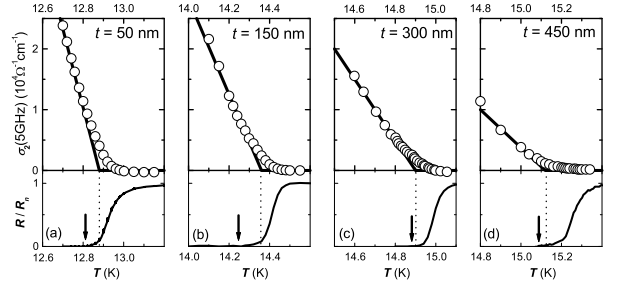


FIG. 4: Temperature dependence of σ_2 at 5 GHz (open circles) and R normalized by the normal resistance, R_n (solid lines in the lower panels). The bold solid lines in the upper panels are the mean-field fitting. The dotted-lines and the arrows indicate T_c^{MF} and T_c^R , respectively.

line is negligible in the range of temperature concerned. With this procedure, the error in the calibrated S_{11} was reduced to 0.01 dB in magnitude, and 0.05° in the phase at 1 GHz.

IV. RESULTS AND DISCUSSION

Figure 3 shows the frequency dependence of complex conductivity of NbN films at several temperatures near T_c . As the temperature approaches T_c from above, both the real part, σ_1 , and the imaginary part, σ_2 , showed a tendency to diverge in the low frequency limit. In addition, a characteristic frequency of $\sigma(\omega)$ decreased, suggesting that the contribution of the superconducting fluctuation to $\sigma(\omega)$ was evident and the relaxation time of the fluctuation became longer.

Figure 4 shows the temperature dependence of σ_2 at 5 GHz, together with the dc resistance, R . Within a mean-field approximation, σ_2 is proportional to the superfluid

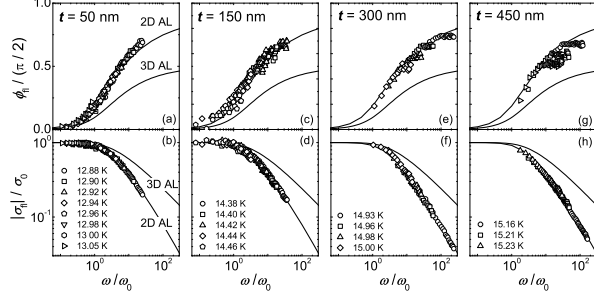


FIG. 5: The results of the dynamic scaling analysis on the phase, ϕ_R , and the magnitude, $|\sigma_R|$ for the NbN films with $t = 50$ nm ((a),(b)), 150 nm ((c),(d)), 300 nm ((e), (f)), and 450 nm((g), (h)). The attempts for the films with $t = 300$ nm and 450 nm were in vain. Here we used the data at $0.4 - 6$, $0.2 - 9$ GHz, $0.3 - 3.5$ GHz, and $0.3 - 3.5$ GHz for the film with $t = 50$ nm, 150 nm, 300 nm, and 450 nm, respectively. The solid lines represent theoretical calculations for 2D-AL and 3D-AL (Eq. (3)). Note that the scaling parameters, ω_0 and σ_0 were derived from these plots.

density, and should vary as $\sigma_2(T) \propto (1 - T/T_c)$ just below T_c , whereas $\sigma_2(T) = 0$ above T_c , as were shown by the bold straight lines in Fig. 4. The experimental data clearly show that the discontinuous superconducting transition changes to a continuous one interconnected by a fluctuation-dominated region. This intermediate region corresponded to the rounding of $R(T)$. In this case, the transition temperature, T_c^{MF} , was determined by the fitting to a mean-field theory, and almost agreed with T_c^R . Rather, T_c^{MF} was a better definition of T_c than T_c^R , since dc resistivity contains the fluctuation-induced finite resistance even below T_c , and is sensitive to a local decrease of T_c owing to, for example, the thickness distribution.

Next, we analyzed the fluctuation conductivity, σ_R , in detail. We subtracted the mean-field conductivity from the total measured conductivity to extract the fluctuation contribution. Here we focused on the fluctuation at $T > T_c$, thus the mean-field conductivity is the normal conductivity, σ_n . Therefore,

$$\sigma_R(\omega, T) \equiv \sigma(\omega, T) - \sigma_n(\omega). \quad (11)$$

Figure 5 shows the result of the scaling of the amplitude, $|\sigma_R|$, and the phase, ϕ_R . For the films with $t = 50$ and 150 nm, the scaled data were in good accordance with the theoretically calculated $S(\omega/\omega_0)$ in the 2D-AL model without the MT-term (Eq. (3)). The absence of the MT-term contribution is reasonable for the dirty films. Contrary to this, the scaling analysis failed for the films with $t = 300$ and 450 nm.

The temperature dependence of the scaling parameters, ω_0 and σ_0 , also confirmed that the observed fluctuation was the 2D-AL fluctuation. Before the quantitative estimation of the critical exponents, it should be noted that the product $\omega_0\sigma_0$ had little temperature dependence

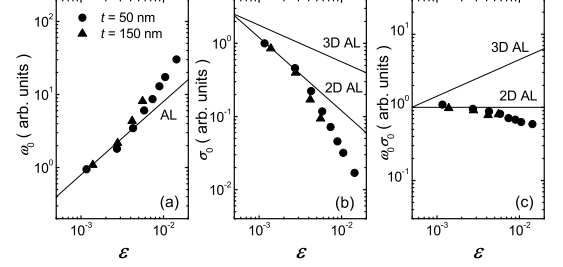


FIG. 6: Temperature dependence of (a) ω_0 , (b) σ_0 , and (c) $\omega_0\sigma_0$, where $\varepsilon = T/T_c - 1$. The solid lines represent theoretical calculation for the 2D-AL model ($\nu = 1/2, z = 2, d = 2$) and the 3D-AL model ($\nu = 1/2, z = 2, d = 3$).

(Fig. 6(c)). This strongly suggested $d = 2$ according to Eq. (6). To obtain the critical exponent, ν and z , T_c has to be determined and ω_0 and σ_0 have to be plotted as a function of $\varepsilon = T/T_c - 1$. We determined T_c^{scale} to obtain the best fit of $\omega_0(\varepsilon)$ and $\sigma_0(\varepsilon)$ to the theoretical prediction. As was also shown in Table I, the obtained T_c^{scale} 's were in fairly good agreement with T_c^{MF} 's. As shown in Fig. 6, $\omega_0(\varepsilon)$ and $\sigma_0(\varepsilon)$ are in good agreement with the 2D-AL fluctuation, in which $\nu = 1/2, z = 2$, and $d = 2$, rather than the 3D-AL fluctuation ($\nu = 1/2, z = 2$, and $d = 3$). The deviation from the theoretical value at higher temperatures is possibly due to the short-wavelength cutoff effects [30]. Here, we should keep in mind that the ambiguity in the choice of T_c^{scale} largely affects the critical exponents. Thus, it is essential to crosscheck if the determined T_c , the critical exponents, and the dimension are consistent with each other in all measurements and analyses. In this study, we obtained the fully consistent data set of $R(T)$, $\sigma_2(T)$, $S(\omega/\omega_0)$, $\omega_0(\varepsilon)$, and $\sigma_0(\varepsilon)$, which yields the identical T_c , the critical exponents, and the dimension.

The observed 2D behavior was apparently puzzling because 3D-AL fluctuation was expected for a three dimensional isotropic superconductor like NbN. We believe that this decrease in the dimensionality stemmed from the size effect. In fact, when $\xi(T) \gg t$, the effective spatial dimension would become 2D. The failure of the dynamic scaling in the thicker films (Fig. 5(e)-(g)) also can be explained by the dimensional crossover due to the size effect because the scaling law is valid only for the limit of 2D or 3D. The effective spatial dimension would change from 3D to 2D as $\xi(T)$ exceeds t when temperatures approaches T_c .

To discuss this size effect more quantitatively, we refer to the calculation of the fluctuation conductivity of thin films with finite thickness by Schmidt [8]. By introducing discrete components of the wave vector normal to the plane of the film, satisfying the boundary condition of vanishing derivative at the surface, the fluctuation

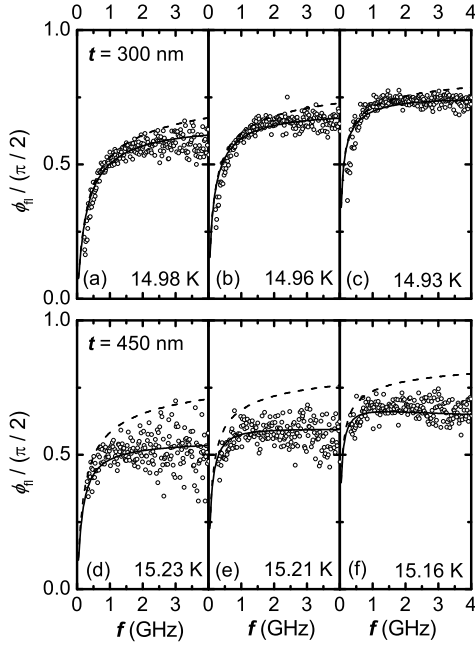


FIG. 7: Frequency dependence of ϕ_H of NbN films with (a)-(c) $t = 300$ nm, and (d)-(f) $t = 450$ nm. The dash lines are the pure 2D calculation (Eq. (3)). The solid lines are the calculation for the case of the dimensional crossover (Eq. (12)).

conductivity was obtained as follows,

$$\sigma(\omega) = \sum_{\nu} \frac{1}{1 + q_{\nu}^2 \xi^2} \sigma^{2\text{DAL}} \left(\frac{\omega}{1 + q_{\nu}^2 \xi^2} \right) \quad (12)$$

$$q_{\nu} = \nu \frac{\pi}{t} \quad \nu = 0, 1, 2, \dots$$

For $\varepsilon \ll \varepsilon_c$ ($\xi \gg t$) only the first term of the series in Eq. (12) gives an appreciable contribution, which is reduced to Eq. (3); contribution from other terms entering for $\varepsilon \sim \varepsilon_c$ or even $\varepsilon > \varepsilon_c$ will spoil the 2DAL-scaling approach. As shown in Fig. 7, $|\phi_H|(\omega)$ of the films with $t = 300$ and 450 nm, can be described by Eq. (12) rather than by the pure 2D formula (Eq. (3)). This indicates that the films cannot be regarded as 2D any longer, suggesting the breakdown of the dynamic scaling behavior.

Although there is no definite criteria to separate the 2D region from the 3D region, we defined a characteristic temperature, $\varepsilon_c = (\pi \xi_0 / t)^2$, by equating $\xi = t / \pi$, below which the pure 2D picture would be expected. In Table I, the estimated values of ε_c are listed. For the films with $t = 50$ and 150 nm, the experimentally observed 2D-AL behavior at temperatures below ε_c is reasonable. On the other hand, for the films with $t = 300$ and 450 nm, the measurement temperatures were in the crossover region from 2D to 3D. In that region, the frequency dependence of σ_H largely changes within the measurement temperature range, so that the data did not collapse to

a unique scaling function. Consequently, the dynamic scaling analysis is inappropriate.

V. CONCLUSION

We measured the frequency and temperature dependences of microwave conductivity of NbN films using a microwave broadband method. We observed the superconducting-fluctuation-induced excess conductivity in the vicinity of T_c . For the films with $t = 50$ and 150 nm, dynamic scaling analysis on fluctuation conductivity yielded 2D-AL behavior. The temperature dependence of R and σ_2 , the obtained scaling function, and the critical exponents were fully consistent. On the other hand, for the films with $t = 300$ and 450 nm, whose sample dimensions were comparable to $\xi(T)$ in the measurement temperature range, the dynamic scaling theory failed to explain the data because of the dimensional crossover. This was an experimental evidence for the breakdown of the scaling behavior owing to the dimensional crossover. These data both validate the dynamic scaling theory and clarify its limits, and serve as a reference for the application of scaling analysis for more exotic superconductors of current interest.

ACKNOWLEDGEMENTS

We thank K. Gomez for useful comments on the manuscript. This work was partly supported by the Grant-in-Aid for Scientific Research (13750005 and 15760003) from the Ministry of Education, Culture, Sports, Science and Technology of Japan. T. Ohashi thanks the Japan Society for the Promotion of Science for financial support.

-
- [1] W. J. Skocpol and M. Tinkham, Rep. Prog. Phys. **38**, 1049 (1975).
 - [2] D. S. Fisher, M. P. A. Fisher, and D. A. Huse, Phys. Rev. B **43**, 130 (1991).
 - [3] B. I. Halperin and P. C. Hohenberg, Phys. Rev. **177**, 952 (1969).
 - [4] J. C. Booth, D. H. Wu, S. B. Qadri, E. F. Skelton, M. S. Osofsky, A. Piqué, and S. M. Anlage, Phys. Rev. Lett. **77**, 4438 (1996).
 - [5] J. Corson, R. Mallozzi, J. Orenstein, J. N. Eckstein, and I. Bozovic, Nature **398**, 221 (1999).
 - [6] S. L. Lehoczky and C. V. Briscoe, Phys. Rev. Lett. **29**, 695 (1969).
 - [7] D. B. Tanner, Phys. Rev. B **8**, 5045 (1973).
 - [8] H. Schmidt, Z. Phys. **216**, 336 (1968).
 - [9] S. Okuma and N. Kokubo, Phys. Rev. B **56**, 14138 (1997).
 - [10] L. G. Aslamazov and A. I. Larkin, Phys. Lett. **26A**, 238 (1968).
 - [11] R. E. Glover, Phys. Lett. **25A**, 542 (1968).
 - [12] K. Maki, Progr. Theoret. Phys. (Kyoto) **39**, 897 (1968).
 - [13] R. S. Thompson, Phys. Rev. B **1**, 327 (1970).
 - [14] M. Strongin, O. F. Kammerer, J. Crow, R. S. Thompson, and H. L. Fine, Phys. Rev. Lett. **20**, 922 (1968).
 - [15] W. E. Masker and R. D. Parks, Phys. Rev. B **1**, 2146 (1970).
 - [16] L. G. Aslamazov and A. A. Varlamov, J. Low Temp. Phys. **38**, 223 (1980).
 - [17] A. T. Dorsey, Phys. Rev. B **43**, 7575 (1991).
 - [18] K. Nakamura, H. Akaike, Y. Ninomiya, Y. Tate, A. Fujimaki and H. Hayakawa, Supercond. Sci. Technol. **14**, 1144 (2001).
 - [19] M. P. Mathur, D. W. Deis, and J. R. Gavaler, J. Appl. Phys. **7**, 3158 (1972).
 - [20] Y. Saito and T. Anayama, J. Appl. Phys. **11**, 5111 (1973).
 - [21] A. Shoji, F. Shinoki, S. Kosaka, and H. Hawakawa, Jpn. J. Appl. Phys. **21** L192 (1982).
 - [22] H. Kitano, T. Ohashi, A. Maeda, and I. Tsukada, Phys. Rev. B **73**, 092504 (2006).
 - [23] S. Maekawa and H. Fukuyama, J. Phys. Soc. Jpn. **51**, 1380 (1981).
 - [24] N. R. Werthamer, E. Helfand, and P. C. Hohenberg, Phys. Rev. **147**, 295 (1966).
 - [25] J. C. Booth, D. H. Wu, and S. M. Anlage, Rev. Sci. Instrum. **65**, 2082 (1994).
 - [26] H. Kitano, T. Ohashi, H. Ryuzaki, A. Maeda, and I. Tsukada, Physica C **412-414**, 130 (2004).
 - [27] See, for example, Agilent Application Note 1287-3 (2002).
 - [28] M. L. Stutzmann, M. Lee, and R. F. Bradley, Rev. Sci. Instrum. **71**, 4596 (2000).
 - [29] D. Karecki, R. E. Peña, and S. Perkowitz, Phys. Rev. B **25**, 1565 (1982).
 - [30] W. L. Johnson, C. C. Tsuei, and P. Chaudhari, Phys. Rev. B **17**, 2884 (1978).